European Cells and Materials Vol.55 2026 (pages 1–16) DOI: 10.22203/eCM.v055a01 ISSN 1473-2262

Original Article

BIOMIMETIC NEUROPEPTIDE Y/COLLAGEN I/β-TRICALCIUM PHOSPHATE SCAFFOLD MEDIATED MACROPHAGE POLARIZATION AND VASCULARIZATION FOR BONE REGENERATION

D.Z. Yang[1,§], Z.C. Chen[1,§], S. Tang[2], J. Tan[1], Z. Xu[1], K. Huang[1], C. He[1], W.H. Yi[1], P. Luo[1,*] and W.D. Han[3,*]

[1]Department of Orthopedics, The 6th Affiliated Hospital of Shenzhen University Health Science Center, 518052 Shenzhen, Guangdong, China
[2]Department of Orthopedics, The 8th Affiliated Hospital of Sun Yat-Sen University, 518000 Shenzhen, Guangdong, China
[3]Department of Pain, The 8th Affiliated Hospital of Sun Yat-Sen University, 518000 Shenzhen, Guangdong, China
[§]These authors contributed equally.

Abstract

Background: Bone grafting is the primary clinical intervention for bone defects. β-tricalcium phosphate (β-TCP) is an absorbable ceramic for its excellent biocompatibility and bioactivity. Neuropeptide Y (NPY) participates in bone homeostasis and vascular regeneration. This research explored the TCP/collagen I (Col)/NPY scaffolds, which controlled release of NPY, on macrophage polarization during bone repair. **Methods**: The scaffold was characterized by scanning electron microscopy (SEM) and Fourier-transform infrared (FTIR) spectrometry. The cumulative NPY release from the TCP/Col/NPY scaffold was tested by an enzyme-linked immunosorbent assay. Biocompatibility of the TCP/Col/NPY scaffold was evaluated using cell counting kit (CCK)-8 and calcein-acetoxymethyl ester (AM)/propidium iodide (PI). Angiogenic activity was detected by scratch and tube-formation assays with human umbilical vein endothelial cells (HUVECs). Osteogenic differentiation was detected by alkaline phosphatase (ALP) staining. Flow cytometry and immunofluorescence staining were used to evaluate RAW264.7 polarization. *In vivo*, bone-defect repair was evaluated using micro-computed tomography scans, hematoxylin and eosin (H&E) staining, Masson and immunohistochemical staining. **Results**: The SEM images disclosed an interconnected pore structure. FTIR of TCP/Col/NPY scaffolds showed a characteristic peak of NPY. The TCP/Col/NPY scaffold exhibited favorable biocompatibility with bone marrow mesenchymal stem cells and promoted the migration and angioenesis of HUVECs. RAW264.7 upregulated cluster of differentiation-206 (CD206) in the TCP/Col/NPY group ($p < 0.05$). *In vivo*, the TCP/Col/NPY scaffold promoted the repair of cranial defects. H&E and Masson revealed that new bone formation in TCP/Col/NPY group was significantly higher ($p < 0.05$). Runx2, osteocalcin, platelet-derived growth factor-BB and CD206/CD80 expression were higher in the TCP/Col/NPY group ($p < 0.05$). **Conclusions**: TCP/Col/NPY scaffolds significantly promoted the repair of critical bone defects by modulating macrophage polarization toward the M2 phenotype and enhancing vascular regeneration.

Keywords: Tricalcium phosphate, neuropeptide Y, bone repair, M2-type macrophages.

***Address for correspondence**: P. Luo, Department of Orthopedics, The 6th Affiliated Hospital of Shenzhen University Health Science Center, 518052 Shenzhen, Guangdong, China. Email: gaidihu0308@sina.com; W.D. Han, Department of Pain, The 8th Affiliated Hospital of Sun Yat-Sen University, 518000 Shenzhen, Guangdong, China. Email: hanwd88@163.com.

Copyright policy: © 2026 The Author(s). Published by Forum Multimedia Publishing, LLC. This article is distributed in accordance with Creative Commons Attribution Licence (http://creativecommons.org/licenses/by/4.0/).

Introduction

Bone defects typically result from trauma, bone tumors, bone infections, congenital malformations, and non-healing fractures [1,2]. Autologous bone is the best choice for bone-defect repair, immune rejection, and disease transmission [3]. However, extraction of autologous bone prolongs the procedure, leading to donor-site complications in 8.5 %–20 % of the patients, and the available quantity of autologous bone is limited [4]. Although allogeneic bone is more easily available than autologous bone, problems related to immune rejection, osteoinduction, disease transmission, and medical ethics have limited its use [5]. Therefore, tissue-engineered bone has become a common method to treat bone defects. However, some problems associated with the use of tissue-engineered bone remain unresolved, including foreign body reactions and poor osteogenic ef-

fects [6]. Recent study has shown that bone regeneration is related to the surrounding microenvironment, and elevated levels of transforming growth factor-β (TGF-β), bone morphogenetic proteins (BMPs), and other biological factors can improve the osteogenic effect [7]. Bone regeneration is also related to nerve and blood vessel regeneration.

Bone homeostasis is regulated by the endocrine and paracrine systems as well as the central and peripheral nervous systems [8]. Neuropeptide Y (NPY), a member of the pancreatic polypeptide family, is a neurotransmitter that regulates bone homeostasis. The biological function of NPY is activated by binding to NPY receptors (Y receptors), including Y1, Y2, Y4, Y5, and Y6 [9]. Y1 and Y2 are key factors regulating bone homeostasis, participating in bone formation and maintaining dynamic bone balance. In the central nervous system, NPY regulates bone metabolism through the Y2 receptor in the hypothalamus. In the peripheral nervous system and bone tissue, NPY regulates bone metabolism through Y1 receptors on the membranes of target cells (such as bone marrow mesenchymal stem cells and osteoblasts) [10]. In bone tissue, high levels of NPY inhibit osteoblastic differentiation and the activity of bone marrow mesenchymal stem cells and reduce bone mass [11]. However, low levels of NPY stimulation in cortical and cancellous bone can increase the activity of osteoblasts and bone mass [12]. In addition, the NPY level is increased in patients with combined brain-fracture injury, suggesting that NPY can directly stimulate mesenchymal stem cells (MSCs), promote their osteogenic differentiation, and help improve bone healing in patients with combined brain-fracture injury [13]. The mechanism underlying the effects of NPY on bone homeostasis is complex, and previous studies have suggested that it is related to the Y1 and Y2 receptors, but some scholars have suggested the opposite [14,15]. Other mechanisms related to NPY may also contribute to its effects on bone metabolism [16].

Macrophages are heterogeneous and plastic and play key roles in maintaining homeostasis and immune regulation. Macrophages can undergo M1 (pro-inflammatory) and M2 polarization (pro-healing) [17]. These two forms of polarization play important roles in regulating homeostasis of the tissue environment [18]. In particular, M2-type macrophages facilitate bone reconstruction and repair functions around the implant material, which can promote bone healing.

In this study, we constructed a β-tricalcium phosphate (β-TCP)/collagen I (Col) (A1048301; Gibco, New York, NY, USA)/NPY microporous scaffold with controlled release of NPY and assessed its slow-release efficiency and biocompatibility. We also evaluated the osteogenic effect of the β-TCP/collagen I/NPY microporous scaffold *in vivo* and investigated the effects of NPY on macrophage polarization and vascular regeneration during endogenous bone repair (Fig. 1).

Materials and Methods

Preparation of Microporous Composite Scaffolds

Neuropeptide Y (P01303; Novoprotein, Suzhou, China) was incorporated into phosphate-buffered saline (PBS) by stirring, yielding a solution with a concentration of 10^{-6} M. Next, 10 μL of the NPY solution (10^{-6} M) was added to 990 μL of collagen I gel (3 mg/mL, A1048301; Gibco, New York, NY, USA), creating a collagen I/NPY mixture with a concentration of 10^{-9} M [12,19]. The β-TCP microporous scaffold (P20221122; DinganTec, Suzhou, China), which was characterized by a cylindrical shape with a diameter of 5 mm and a height of 2 mm, was treated with 150 μL of the collagen I/NPY mixture. This step was performed in 5-mm-diameter dishes at a low temperature of 4 °C for 2 h, followed by 24 h incubation in a vacuum-negative pressure freezer to produce the β-TCP/collagen I/NPY microporous scaffold. Additionally, 150 μL of collagen I gel was combined with the β-TCP microporous scaffold under identical conditions, yielding the β-TCP/collagen I microporous scaffold. The scaffold composed of β-TCP and collagen I was referred to as TCP/Col, while that containing β-TCP, collagen I, and NPY was labeled as TCP/Col/NPY. Furthermore, the β-TCP scaffold alone was designated as TCP.

Characterizations of the Microporous Composite Scaffolds

Morphological characteristics of the surfaces and cross-sections of the TCP, TCP/Col, and TCP/Col/NPY microporous scaffolds were observed using scanning electron microscopy (SEM). After spraying gold onto the sample surface, the TCP, TCP/Col, and TCP/Col/NPY microporous scaffold surfaces were placed in the electron microscope sample compartment of a scanning electron microscope (EVO 18; ZEISS, Germany) and observed under vacuum conditions at different magnifications. The mechanical properties of the scaffolds were evaluated using a mechanical testing instrument (M6000; CARE, Tianjin, China), and the load-displacement curves were recorded continuously. A Thermo Fisher Nicolet iS5 Fourier-transform infrared (FTIR) spectrometer (Waltham, MA, USA) was used to identify functional groups and chemical interactions. The microporous scaffolds were compressed into a potassium bromide (KBr) disc and evaluated in absorption mode at a resolution of 4 cm^{-1} with 32 scans in the 650–4000 cm^{-1} range.

Evaluation of Cumulative Release of NPY from Microporous Composite Scaffolds

The prepared TCP/Col/NPY microporous scaffolds were added to centrifuge tubes with 1 mL of PBS and kept at 37 °C. The PBS was changed daily for the first week, followed by removal at 10, 15, and 20 d. The NPY content of the PBS solution was measured using an NPY enzyme-linked immunosorbent assay (ELISA) kit (D711352; Sangon, Shanghai, China).

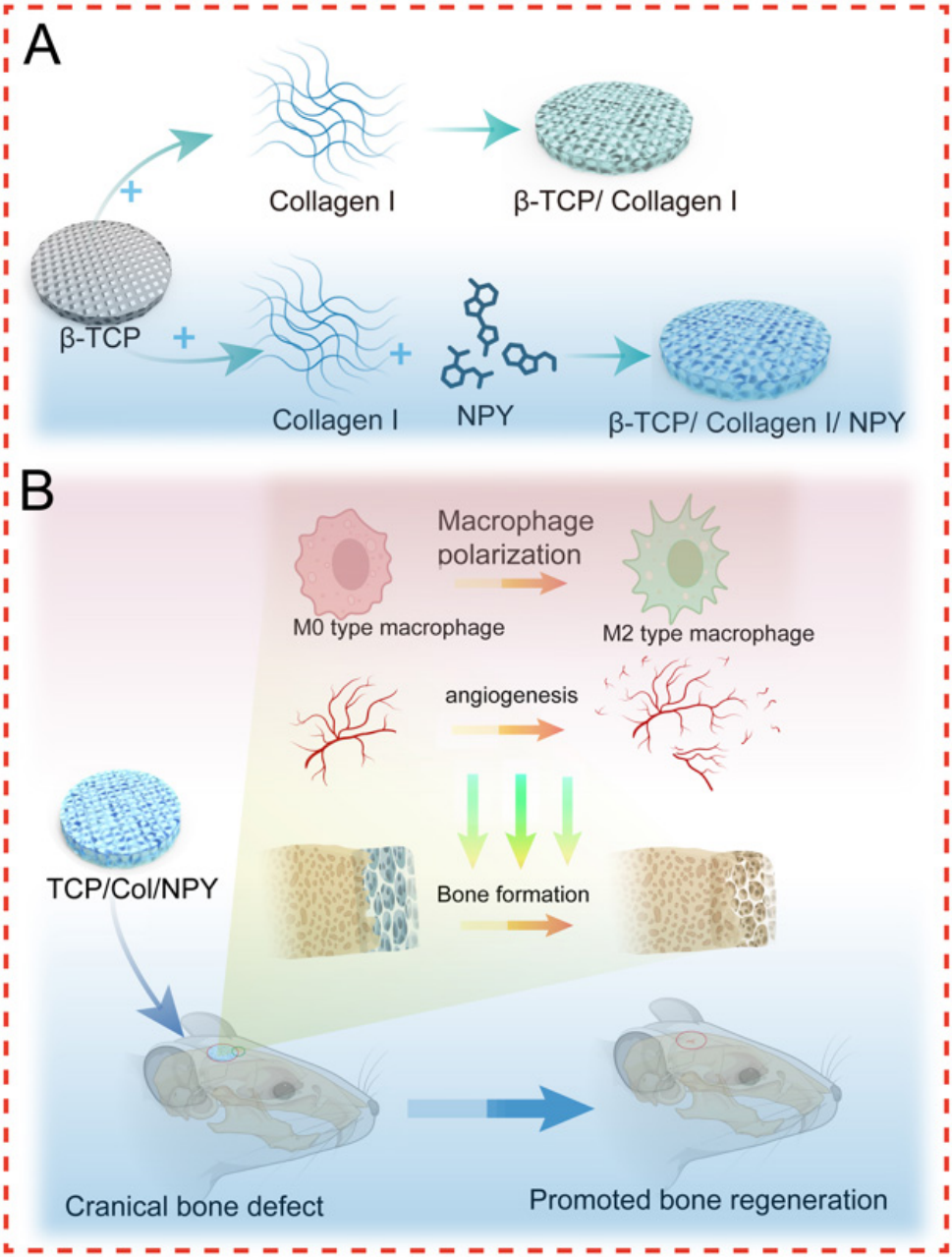

Fig. 1. Graphical illustration of this study. (**A**) Fabrication of the microporous scaffold with β-TCP, collagen I, and NPY. (**B**) Biological evaluation of the microporous scaffold *in vitro*, where M2 macrophage polarization and enhanced angiogenesis are observed, and successful bone regeneration of rats is achieved by the microporous scaffold *in vivo*. Created with Adobe Illustrator and Created in BioRender. Chen, Z. (2025) https://BioRender.com/24tr539.

Cell Culture

Sprague-Dawley rat bone marrow MSCs (SD-BMSCs) were obtained from Shanghai Zhong Qiao Xin Zhou Biotechnology (ZQY122, CELL RESEARCH, Shanghai, China). The SD-BMSCs were cultured in Dulbecco's modified Eagle medium (DMEM; Hyclone, SH30022.01; Logan, UT, USA) supplemented with 10 % fetal bovine serum (A5670801; Gibco, New York, NY, USA) and 1 % penicillin (60162ES; Yeasen Biotech, Shanghai, China). Mouse RAW264.7 cells were sourced from Procell Life Science & Technology (CL-0190; Wuhan, China) and were cultured in DMEM (Hyclone, SH30022.01; Logan, UT, USA) with 10 % fetal bovine serum (Gibco, A5670801, New York, NY, USA) and 1 %

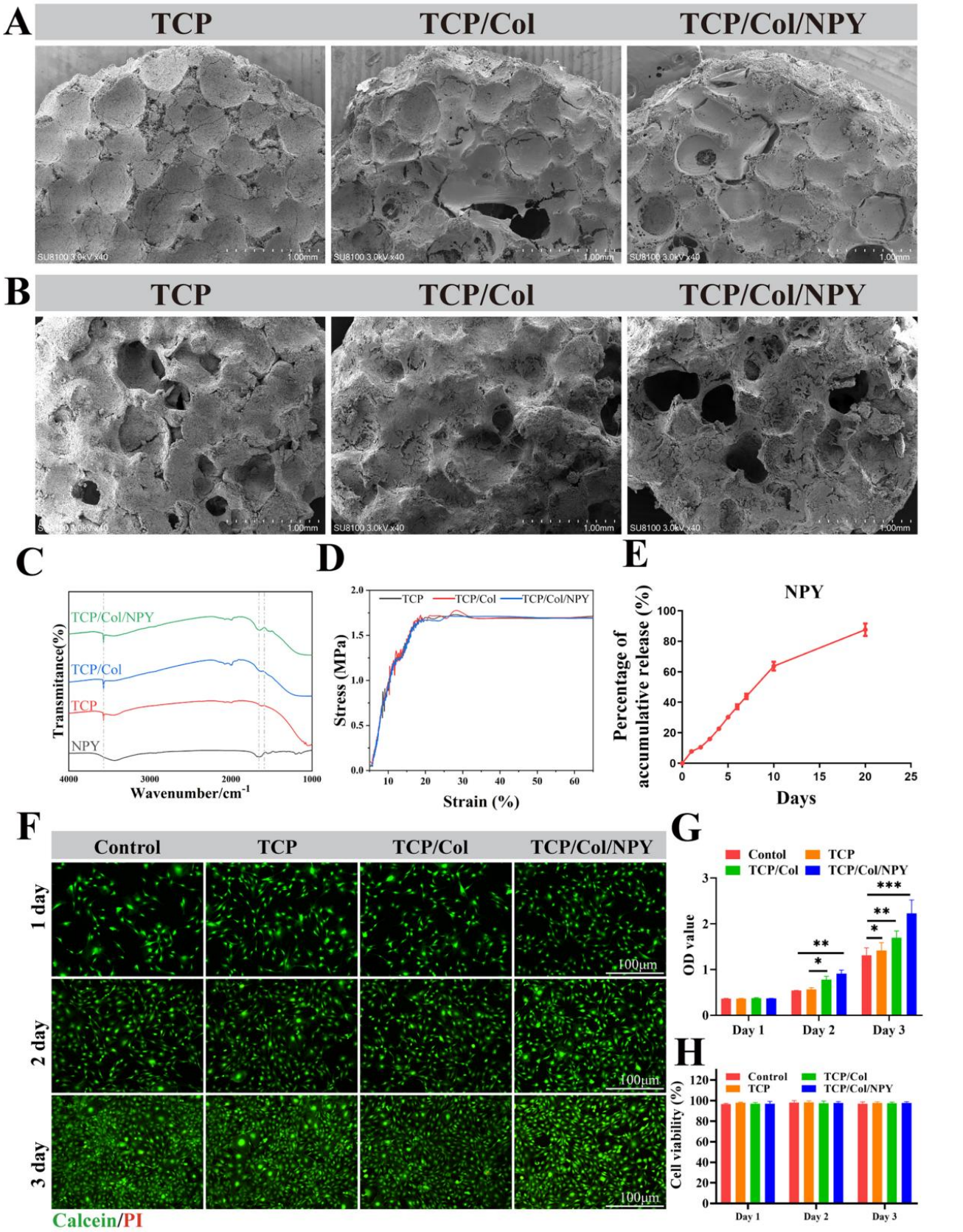

Fig. 2. Characterization and biocompatibility assessment of the microporous scaffolds. (**A**) SEM image. (**B**) SEM image with cells. (**C**) Fourier-transform infrared spectra. (**D**) Mechanical performance of the microporous scaffolds. (**E**) Release profiles of the microporous scaffolds. (**F**) Calcein-AM/PI staining of BMSCs, alive (green stain), dead cells (red stain). (**G**) Cell proliferation evaluated by the CCK-8 assay. (**H**) Survival rate. *$p < 0.05$, **$p < 0.01$, ***$p < 0.001$. ns, $p > 0.05$.

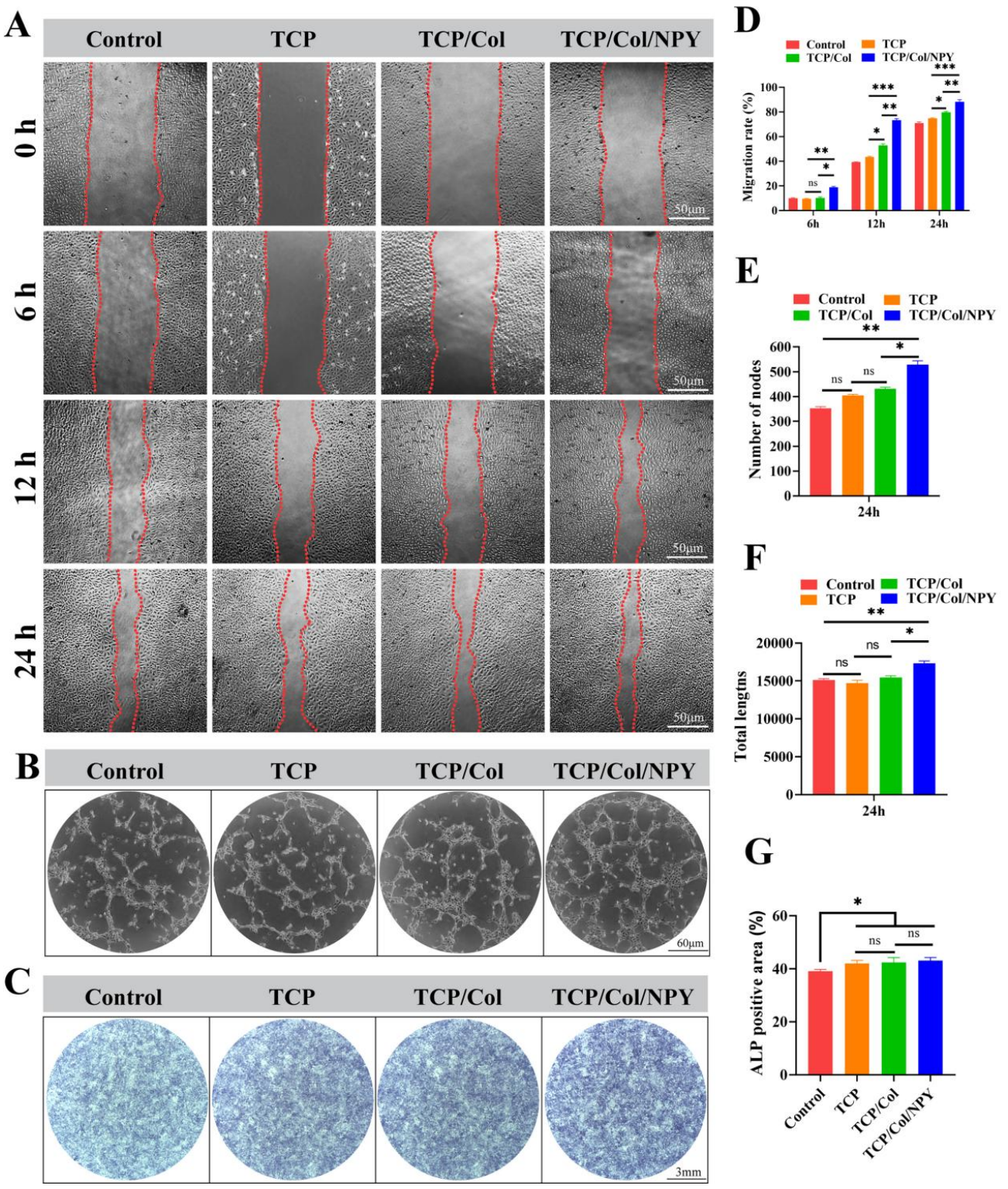

Fig. 3. Evaluation of the angiogenic and osteogenic effects of the microporous scaffolds *in vitro*. (**A**) Scratch assay. (**B**) Tube-formation assay. (**C**) ALP staining results. (**D**) The quantification data of the migration rate showed in **A**. (**E**) Number of nodes showed in **B**. (**F**) The quantification data of the total length showed in **B**. (**G**) The quantification data of ALP positive area showed in **C**. *$p < 0.05$, **$p < 0.01$, ***$p < 0.001$. ns, $p > 0.05$.

penicillin (Yeasen Biotech, 60162ES; Shanghai, China). Human umbilical vein endothelial cells (HUVECs) were purchased from Procell Life Science and Technology (CL-0675; Wuhan, China). Cells were grown in complete culture medium for PUMC-HUVEC-T1 (Pricella Life Science & Technology Co., Ltd., CM-0675, Wuhan,

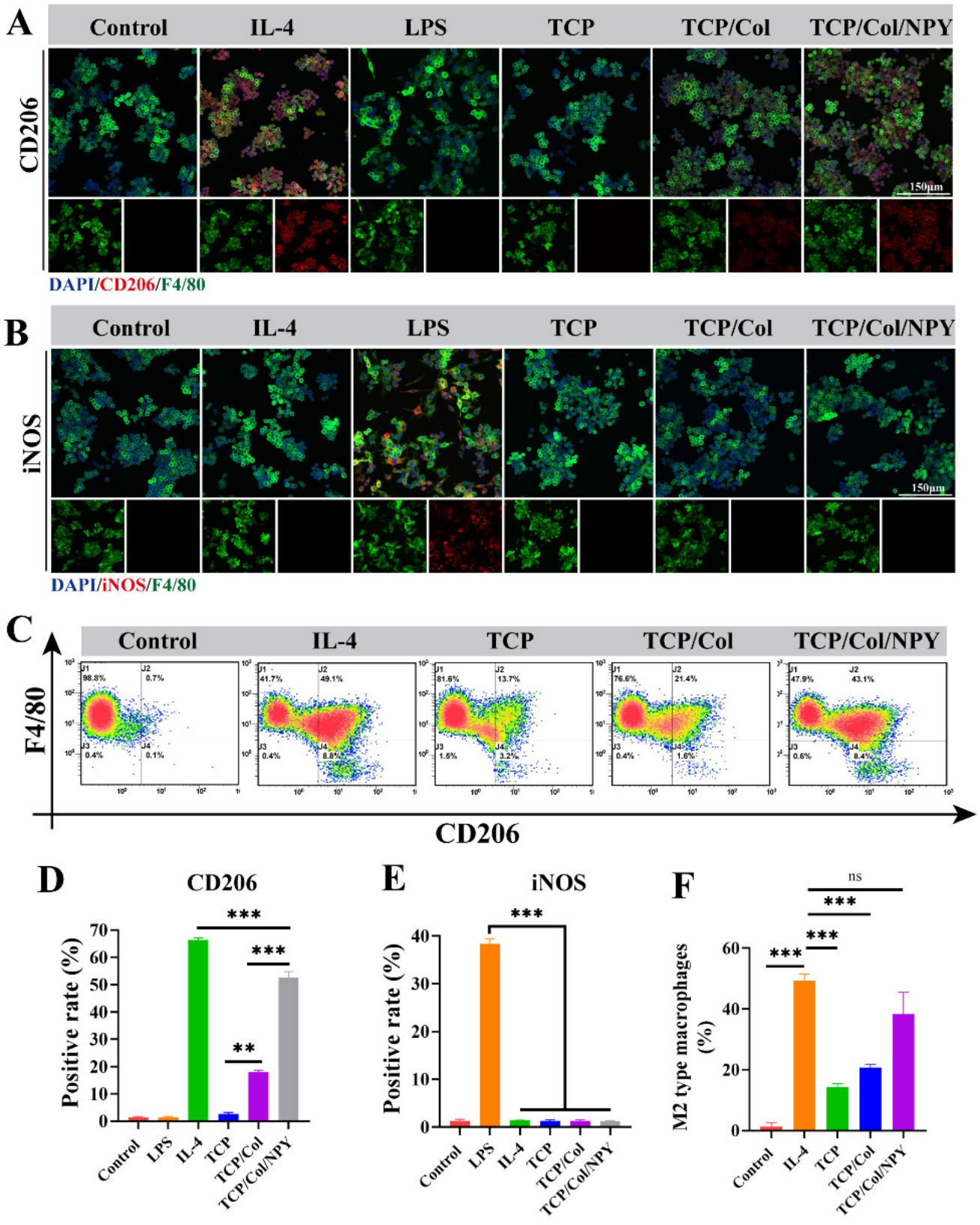

Fig. 4. Inflammatory response of macrophages on the microporous scaffolds *in vitro*. (**A,B**) Immunofluorescence and statistical analyses of CD206 (**D**) and iNOS (**E**). (**C**) Flow cytometry analysis of CD206 and F4/80. (**F**) Percentages of M2-type macrophages quantified by flow cytometry: three independent experiments (n = 3), with error bars representing standard error (SE). *$p < 0.05$, **$p < 0.01$, ***$p < 0.001$. ns, $p > 0.05$.

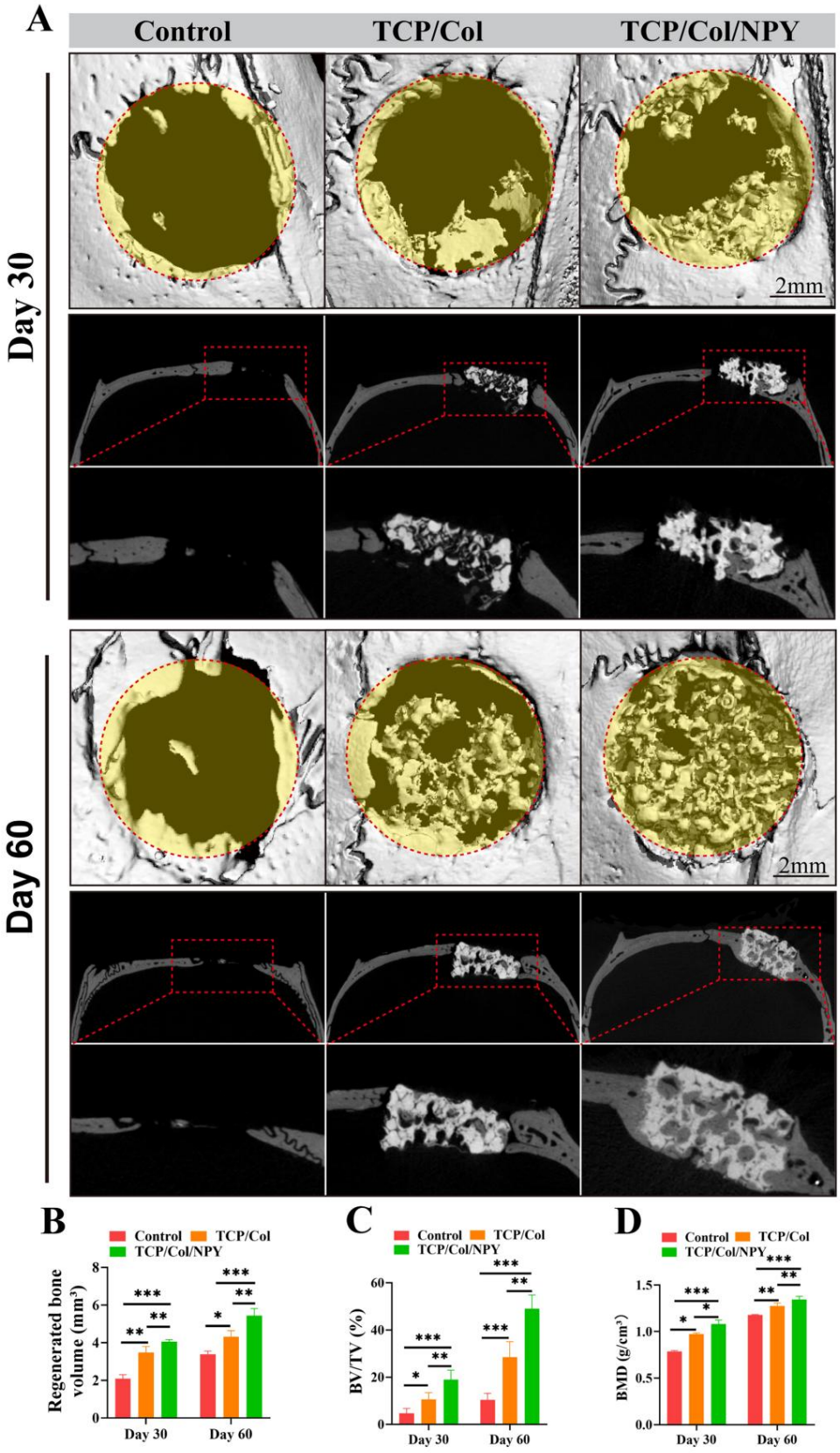

Fig. 5. Bone regeneration efficacy of the microporous scaffolds implanted in rats *in vivo*. (**A**) Micro-CT scans pictures of the samples in the rat cranial defect model on day 30 and day 60. (**B–D**) The statistical histogram of regeneration bone volume (**B**), BV/TV (**C**), and BMD (**D**). BV, bone volume; TV, total volume; BMD, bone mineral density. *$p < 0.05$, **$p < 0.01$, ***$p < 0.001$. ns, $p > 0.05$.

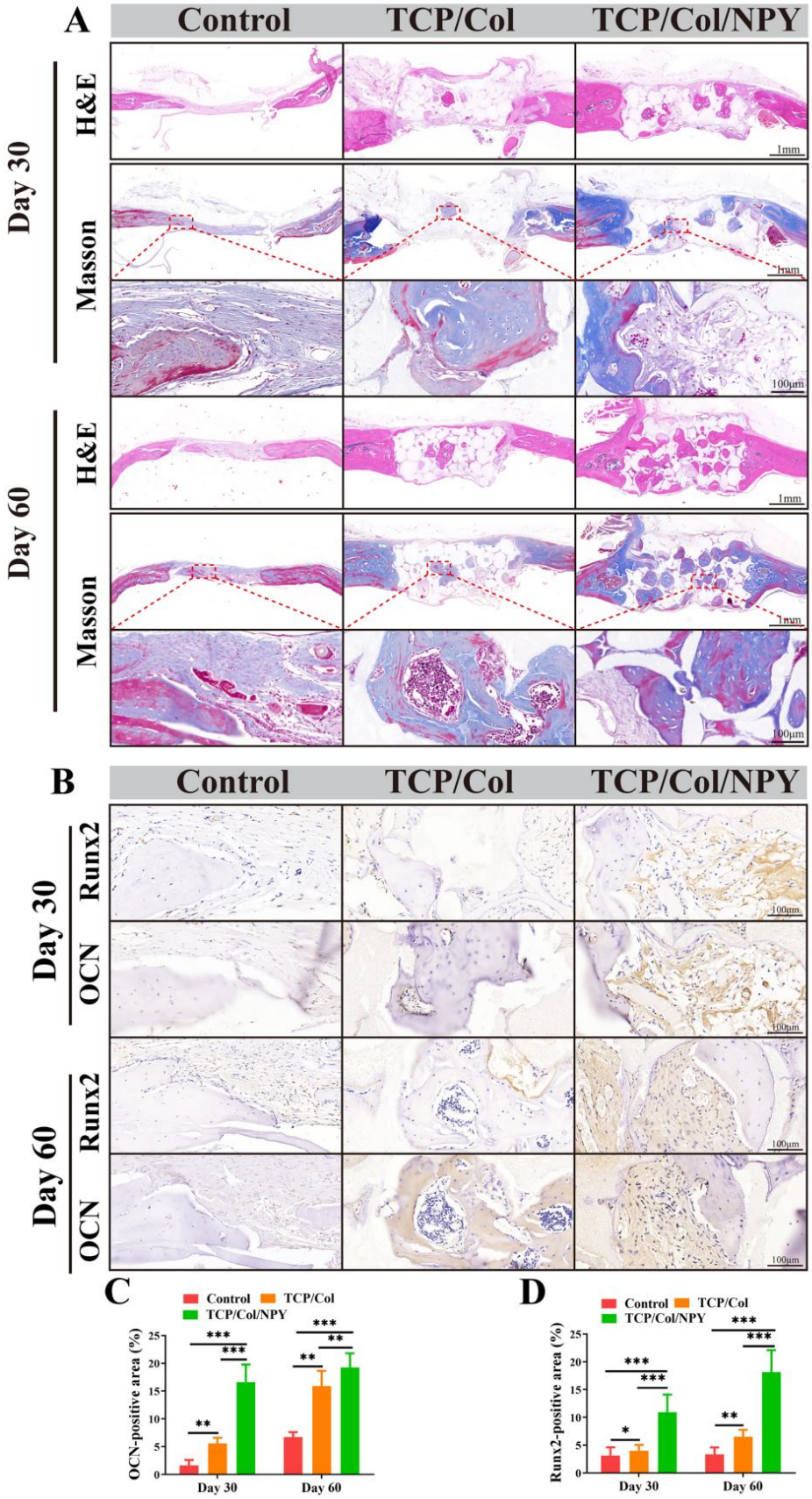

Fig. 6. Osteogenic evaluation of the microporous scaffolds *in vivo*. (**A**) H&E staining and Masson's trichrome staining. (**B**) Immunohistochemical staining of OCN and Runx2. (**C,D**) The statistical histogram of OCN-positive area showed in **B** (**C**) and Runx2-positive area showed in **B** (**D**). *$p < 0.05$, **$p < 0.01$, ***$p < 0.001$. ns, $p > 0.05$.

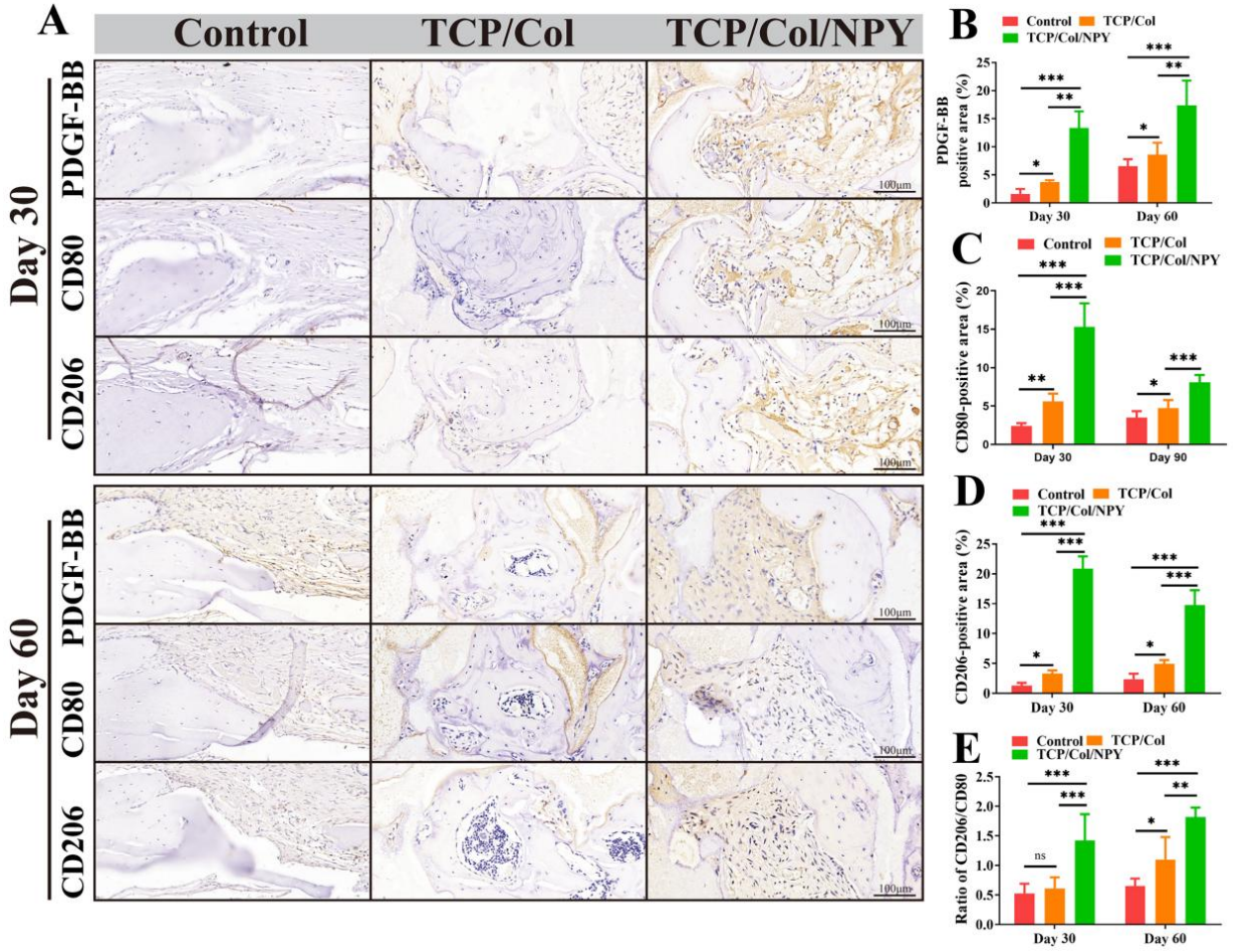

Fig. 7. The immunomodulatory activity of the microporous scaffolds *in vivo*. (**A**) The Immunochemical staining of PDGF-BB, CD206, and CD80. (**B–E**) The statistical results PDGF-BB-positive area (**B**), CD80-positive area (**C**), CD206-positive area (**D**) and ratio of CD206/CD80 (**E**) showed in **A**. *$p < 0.05$, **$p < 0.01$, ***$p < 0.001$. ns, $p > 0.05$.

China). All cells were incubated at 37.5 °C in a 5 % CO_2 environment, with the medium changed every three days. The SD-BMSCs, RAW264.7 cells and HUVECs were performed with mycoplasma test and confirmed that the mycoplasma did not exist in all groups.

Cell Compatibility of the Microporous Composite Scaffolds

SD-BMSCs were seeded onto the TCP, TCP/Col, and TCP/Col/NPY microporous scaffolds at a density of 4 × 10^3 cells per sample with 96-well plates as the holders. After 48 h, fixation with an electron microscope fixative was performed, and SEM was used to observe the morphological characteristics of the cells on the microporous scaffolds. In the SEM process, the samples were lyophilized, sputter-coated with gold, and examined using an EVO 10 SEM device (ZEISS, Germany) with an accelerating voltage of 20.0 kV.

The TCP, TCP/Col, and TCP/Col/NPY microporous scaffolds were added in DMEM in a 37.5 °C thermostat (ratio of the mass of the samples go to the volume of the culture medium: 1:10). The extracts were collected after three days and filtered through a 0.22-μm pore membrane. The SD-BMSCs (5 × 10^3) were seeded in 96-well plates, and the material extract medium was added after 24 h. Cell proliferation was examing by a cell counting kit assay (CCK-8, 40203ES; Yeasen Biotech, Shanghai, China) according to the manufacturer's protocol. After incubating with the CCK-8 reagent for 30 min at 37 °C, the medium of each group was measured using a microplate reader (Biotek Synergy H1; Thermo Scientific, Waltham, MA, USA) at wavelength of 450 nm.

A live/dead assay was conducted to assess the cytotoxicity of the scaffolds. SD-BMSCs (1 × 10^4) were seeded in 24-well plates; the material extract medium was added after 24 h; the cells were stained with calcein-acetoxymethyl ester (AM) and propidium iodide (PI) following the manufacturer's protocols (C2015S; Beyotime, Shanghai, China); and the live/dead cells were visualized under a confocal laser scanning microscope (CLSM, FV3000; Olympus, Tokyo, Japan).

In Vitro Angiogenesis

A scratch assay was performed to evaluate the effects of the extract on endothelial cell function. HUVECs were trypsinized and seeded in 12-well plates with 1 mL of serum-free medium per well. The center of each well in the 12-well plate was scratched with a 200-μL pipette tip, observed, and photographed under an optical microscope. Different extraction media were subsequently added. After 24 h, cell healing in each group was observed using an optical microscope and documented with photographs. ImageJ software (1.8.0; NIH, Bethesda, MA, USA) was utilized to calculate the scratch area, with the cell migration rate of the control group set as 100 % to calculate the migration rates of the test groups.

A tube-formation assay was performed to evaluate the tube-formation capacity of the material extract media in vascular endothelial cells. Cells (2×10^5) were plated onto a 12-well plate on a reconstituted basement membrane (Low Growth Factor Matrigel; 356230; BD Biosciences, San Jose, CA, USA), and endothelial cell-tube over 6–8 h after cell seeding was observed and photographed under an inverted microscope. The number, nodes, and branches of angiogenesis were analyzed using ImageJ software.

In Vitro Osteogenesis Study

SD-BMSCs were seeded on a 12-well plate, and osteogenic differentiation was induced by culturing with osteogenic medium (Cyagen, RAXMX-90021; Suzhou, China) mixed 1:1 with the extracts of the microporous scaffolds. The culture medium was replaced every three days. After approximately eight days, the cells in the various groups were fixed in a 4 % paraformaldehyde solution and stained using an alkaline phosphatase (ALP) staining kit (Beyotime, P0321S; Shanghai, China). The stained cells were observed under a light microscope (Olympus, IX70; Tokyo, Japan) and analyzed using ImageJ 1.8.0.

In Vitro Responses of Macrophages

RAW264.7 cells were seeded onto 35-mm confocal dishes at a density of 1×10^3 cells and maintained in DMEM with 10 % fetal bovine serum and 1 % penicillin/streptomycin at 37 ℃. This medium was mixed with extracts of the microporous scaffolds in a 1:1 ratio and refreshed every two days. After two days, the cells were fixed with 4 % paraformaldehyde, permeabilized using 0.1 % Triton-X100, and blocked with 5 % goat serum. Afterwards, the cells were co-incubated overnight at 4 °C with primary antibodies against inducible nitric oxide synthase (iNOS) (1:150 dilution, ab178945; Abcam, Cambridge, UK), F4/80 (1:150 dilution, ab6640; Abcam), and mannose receptor (CD206) (1:150 dilution, ab300621; Abcam). An additional 1-hour incubation at room temperature was performed using Alexa Fluor 488 goat anti-rabbit (1:1000 dilution, ab150077; Abcam) and Alexa Fluor 594 goat anti-rat (1:1000 dilution, ab150160; Abcam) antibodies. Subsequently, the cells from the various groups were stained with 4',6-diamidino-2-phenylindole and covered with a coverslip. Immunofluorescence of the cells was assessed via a CLSM (FV3000; Olympus, Tokyo, Japan) and analyzed with ImageJ 1.8.0 software.

Flow cytometry was utilized to evaluate the RAW264.7 macrophages. The RAW264.7 cells were seeded in 6-well plates at a density of 1×10^5 cells/well. The medium was mixed in a 1:1 ratio with extracts of the microporous scaffolds and refreshed every two days. After two days, the harvested cells were washed with PBS to remove the culture medium. The cells were stained with phycoerythrin (PE)-linked anti-F4/80 (12-4801-82; eBioscience, San Diego, CA, USA) and Alexa Fluor 488-linked anti-CD206 (53-2061-82; eBioscience) for 1 h at room temperature. Stained cells were washed with and resuspended in PBS. Flow cytometry was performed using the Navio device (B47903; BECKMAN COULTER, Navios, Brea, CA, USA), and the results were analyzed using ImageJ software (1.8.0; NIH, Bethesda, MA, USA).

Implantation of Microporous Scaffolds in Rat Cranial Defects

The Guangdong Provincial Experimental Animal Center supplied eighteen male Sprague-Dawley rats. The subjects were male Sprague-Dawley rats, 8 weeks old, and weighing 250–300 g. The rats were kept in the environment within a temperature of 21 °C ± 2 °C and 12 h light/dark cycle. They were provided with free access to food and water. To establish the cranial defect model, the rats were intraperitoneally anesthetized with pentobarbital sodium (60 mg/kg), and the dorsal cranium was exposed. A high-speed drill with a trephine burr was utilized to make a 5-mm-diameter defect. Saline was used to flush each defect for removing bone debris, followed by the implantation of the scaffolds. Eighteen male Sprague-Dawley rats were randomly assigned into three groups: empty-defect group (n = 6), TCP/Col group (n = 6), and TCP/Col/NPY microporous scaffold group (n = 6). Subsequent to the implantation of the biomaterials, the soft tissues were sutured using skin staples, and the rats were allowed to perform free activity in the cages. At 30 and 60 d, three rats in each group were euthanized.

Micro-Computed Tomography Scan

Whole-cranial samples of Sprague-Dawley rats were scanned using micro-computed tomography (micro-CT; μCT100; SCANCO Medical AG, Brüttisellen, Switzerland). The scanning parameters were as follows: voltage, 70 kV; current, 200 μA; 0.5 mm aluminum foil filter; scan angle, 180°; rotation step length, 0.18°; scan voxel size, 17.2 μm; 2048 × 2048 × 400. Three-dimensional (3D) reconstruction of the two-dimensional (2D) (Skyscan CTAn, Bruker, Kontich, Belgium) images obtained after scanning was performed using SCANCO μCT Evaluation Program

V6.6. During reconstruction, a bone gray threshold value of 220–450 was selected using the software, and the microporous scaffold at the defect was removed (microporous scaffold gray value >450).

Hematoxylin and Eosin and Masson Staining

A 10 % ethylenediaminetetraacetic acid (EDTA) solution (Solarbio, E1171, Beijing, China) was used to decalcify the cranial specimen, and the solution was replaced with a new 10 % EDTA solution every two days. One month later, all cranial specimens were embedded in paraffin and sectioned at 5 μm. After dewaxing and dehydration, hematoxylin and eosin (H&E) and Masson's trichrome staining were executed in accordance with protocols. Histological slides were scanned (20×) using Pannoramic SCAN II (3DHISTECH, SCAN II; Budapest, Hungary). Images of the scanned stained slides were obtained using the CaseViewer system (v2.0.X; 3DHISTECH, Budapest, Hungary).

Immunohistochemical Analyses

The samples were embedded in paraffin and sectioned at 5 μm, as described previously. After deparaffinization and dehydration, the Histostain-Plus IHC Kit (859043; Invitrogen, New York, NY, USA) was used for immunohistochemical staining. The experiments were performed according to the manufacturer's protocol. Histological slides were scanned (20×) using Pannoramic SCAN II (3DHISTECH, Budapest, Hungary). Images of the scanned stained slides were analyzed using the CaseViewer system (3DHISTECH, Budapest, Hungary). ImageJ software was used to analyze and calculate the percentage of the area covered by cells showing positive signals for Runx2 (8486S; CST, Danvers, MA, USA), osteocalcin (OCN; ab111250; Abcam, Cambridge, UK), CD80 (ab134120, Abcam, Cambridge, UK), CD206 (24595; CST, Danvers, MA, USA), and platelet-derived growth factor-BB (PDGF-BB; ab21234; Abcam, Cambridge, UK).

Statistical Analyses

Experimental data were statistically analyzed using SPSS 24.0 (IBM Corp., Armonk, NY, USA). Data were tested for normality distribution using D'Agostino and Pearson normality testing. The statistical significance of the differences between two groups was evaluated using Student's *t*-test. The data were presented as the mean ± standard deviation (SD), and $p < 0.05$ indicated that the difference was statistically significant.

Results

Characteristics of the NPY Microporous Scaffold

SEM images showed that the microporous scaffolds retained the interconnected pore structure of TCP. As shown in Fig. 2**A**, due to the loading of collagen I, the TCP/Col and TCP/Col/NPY scaffolds were relatively smooth. Fourier-transform infrared (FTIR) analysis provided further insights into the chemical functional groups on the sample surfaces. All samples exhibited distinct absorption bands at 3570, 1644, and 1544 cm^{-1}, which corresponded to vibrational modes of -OH, C=C, N=O. In contrast, NPY presented characteristic peaks at 1644 and 1544 cm^{-1}, which were respectively related to C=C and N=O. The results for the TCP/Col/NPY scaffolds revealed additional absorption bands at 1644 and 1544 cm^{-1}, representing C=C and N=O (Fig. 2**C**). These results suggested successful integration of NPY into the microporous scaffolds.

The mechanical assessments indicated that the stress-strain curve was essentially consistent across the three groups, and collagen I and NPY loading did not change the mechanical properties of the β-TCP scaffold (Fig. 2**D**).

Release Rate of NPY

To explore the release rate of NPY from the TCP/Col/NPY microporous scaffold, we first determined the total drug loading of NPY in the TCP/Col/NPY microporous scaffold using ELISA. The average drug loading on each 10-mg scaffold sample was 321.76 ± 30.58 pg. ELISA was then performed to detect the concentration of NPY released from the TCP/Col/NPY microporous scaffold in the PBS solution at 12 h, 24 h, 2 d, 3 d, 4 d, 5 d, 7 d, 10 d, and 15 d, and the cumulative release rate of NPY was calculated. These results showed that NPY was compounded by the TCP/Col scaffold and released continuously for 20 days in an aqueous solution. The cumulative release rate at 10 d was 63.70 % ± 3.98 %, and that at 20 d was 87.62 % ± 5.57 % (Fig. 2**E**).

Biocompatibility with the Microporous Scaffold

Although the concept is somewhat controversial, biocompatibility refers to the successful interaction between living biological tissues and nonliving materials. To explore the cytotoxicity of the microporous scaffold, SD-BMSCs were incubated onto the microporous scaffolds. Subsequent to a 48-hour period, the majority of cells that had adhered to different scaffolds were viable, and the cells exhibited a stretched morphology on SEM images (Fig. 2**B**). Calcein-AM/PI staining indicated that BMSCs underwent robust proliferation on the cell plates, and most of the cells were alive (green stain), with a few dead cells (red stain) from days 1 to 3 (Fig. 2**F**). The survival rate did not differ significantly among the groups ($p > 0.05$) (Fig. 2**H**). Furthermore, the CCK-8 assay showed that cells proliferated in all groups. In particular, the TCP/Col/NPY microporous scaffolds effectively promoted cell proliferation (Fig. 2**G**). This finding indicated that the biocompatibility of these microporous scaffolds was excellent.

In Vitro Angiogenic Behavior

Angiogenesis plays a critical role in the regeneration of bone defects. In this study, the effectiveness of microporous scaffolds in stimulating angiogenesis was assessed using tube-formation and HUVEC-migration assays. In the tube-formation assays, the TCP/Col/NPY group outperformed the other three groups in both the number of nodes and total length ($p < 0.05$) (Fig. 3**B,E,F**). Moreover, the HUVEC-migration tests indicated that cells migrated more rapidly in the TCP/Col/NPY group at both 24- and 48-h intervals in comparison with the other groups ($p < 0.05$) (Fig. 3**A,D**). These results demonstrate that the TCP/Col/NPY microporous scaffold could effectively promote angiogenesis.

In Vitro Osteogenic Behavior

The osteogenic capacity of the microporous scaffolds is of great significance for bone regeneration materials. Neuropeptide Y (NPY) has been demonstrated to promote the migration and osteoblastic differentiation of mesenchymal stem cells (MSCs) and accelerate fracture healing. In our study, on day 8, SD-BMSCs showed ALP-positive staining in all groups; however, the TCP, TCP/Col, and TCP/Col/NPY groups exhibited stronger ALP staining compared to the control group ($p < 0.05$). No significant differences in expression were observed among the TCP, TCP/Col, and TCP/Col/NPY groups ($p > 0.05$; Fig. 3**C,G**).

Inflammatory Response of Macrophages

Polarized macrophages are classified as either M1 or M2 cells, according to the T helper cell 1/2 (Th1/Th2) nomenclature. In our study, the immunomodulatory ability of the microporous scaffold was assessed using RAW264.7 cells, which were cultured in extracts derived from the scaffolds for 48 h. CD206 is a maker indicative of the anti-inflammatory M2 phenotype, and immunofluorescence staining for CD206 showed a significant predominance of M2 macrophages in TCP/Col/NPY group than in the TCP and TCP/Col groups ($p < 0.05$; Fig. 4**A,D**). Moreover, the expression level of iNOS, a marker for the pro-inflammatory M1 macrophage phenotype, remained low in three scaffolds groups compared to lipopolysaccharides (LPS) groups (Fig. 4**B,E**), indicating that none of the scaffolds elicited a substantial inflammatory response. Furthermore, flow cytometry analysis showed that the macrophages in the TCP/Col/NPY scaffold group upregulated CD206 expression (Fig. 4**C,F**). These results suggest that the TCP/Col/NPY scaffold has the intrinsic ability to re-culture macrophages from the M0 to the M2 phenotype.

TCP/Col/NPY Microporous Scaffold Promotes Repair of Cranial Defects in Sprague-Dawley Rats

In the rat defect model, at 30 d, micro-CT scanning revealed almost no bone formation in the control group, whereas the TCP/Col group showed a small amount of bone formation at the edge of the bone defect, and the TCP/Col/NPY group showed a larger amount of bone formation. At 60 d, the cranial defects were largely repaired in the TCP/Col/NPY group, whereas the TCP/Col group showed significantly less new bone. Continuous bone formation was not observed in the empty-defect group ($p < 0.05$; Fig. 5**A**). At both 30 and 60 d, the bone volume (BV)/total volume (TV) and new bone formation area in the TCP/Col/NPY group were significantly higher compared to the other groups ($p < 0.05$; Fig. 5**B–D**).

After 30 d, H&E and Masson staining indicated that, within the control group, the bone defect was filled with soft connective tissue, and no bone structure formation was observed. However, in the TCP/Col/NPY group, more new bone was observed in the scaffolds. At 60 d, these differences were even more pronounced (Fig. 6**A**). At 30 d, immunohistochemical staining showed that in the connective tissue surrounding the new healing bone, the Runx2/OCN protein ratio in the TCP/Col/NPY group was significantly higher than that in the TCP/Col and control groups ($p < 0.05$). At 60 d, these differences were even more significant ($p < 0.05$; Fig. 6**B–D**).

NPY Microporous Scaffold Promoted the Expression of PDGF-BB and Molecules Associated with M2-Type Macrophages

At day 30, PDGF-BB was highly expressed in both the TCP/Col and TCP/Col/NPY groups, and PDGF-BB expression gradually increased over time ($p < 0.05$). The expression levels of CD80 and CD206 were high at 30 d and low at 60 d in the TCP/Col and TCP/Col/NPY groups. However, after 60 d, the CD80 expression in the TCP/Col/NPY group was significantly reduced than that in the TCP/Col group ($p < 0.05$). The CD206/CD80 ratio increased from day 30 to 60. A significantly elevated CD206/CD80 ratio was observed in the TCP/Col/NPY group compared to other groups ($p < 0.05$; Fig. 7**A–D**).

Discussion

Bone regeneration is a complex physiological process that involves immune responses, angiogenesis, osteogenesis, and other steps [20,21]. Bone regeneration is related to nerve and blood vessel regeneration [22]. Study has shown that innervation of bone defects offers great potential for sequential regulation of the bone microenvironment. Early innervation of the bone-defect area is essential for bone healing progression from inflammation to fibrovascular phase. During the fibrovascular phase of bone healing, nerve regeneration exhibits a strong correlation with angiogenesis in bone healing [23].

Neurotransmitters and neuropeptides such as vasoactive intestinal peptide, substance P, calcitonin gene-related peptide, and NPY are involved in bone regeneration [24, 25]. The mechanisms of action of neurotransmitters and

neuropeptides remain unclear and may be related to angiogenesis during bone healing. NPY is principle regulators of bone homeostasis and plays a crucial role in bone homeostasis [26]. NPY expression shows an increasing trend throughout the fracture-healing process. NPY levels are elevated in the initial stages of fracture, and during this phase [27], NPY is mainly involved in inflammatory reactions and callus formation related to fracture hematoma [28]. During the inflammatory phase, NPY can activate the receptors of immune cells, including white blood cells, antigen-presenting cells, and macrophages [29]. In the middle and late stages of fracture, NPY is mainly involved in the regulation of bone remodeling. Paradoxically, several studies have found that low dosages of NPY promote the osteogenic differentiation and mineralization of BMSCs, whereas a high NPY concentration exerts the opposite effect [30,31]. In this study, we combined low doses of NPY (10^{-9}M) with β-TCP/collagen I to explore the effect of the NPY microporous scaffold on bone-defect repair. Firstly, the micropore diameter of the TCP/Col/NPY scaffold was 150–300 μm, which was conducive to the entry of cells and the growth of tissues [32]. FTIR analysis of the TCP/Col/NPY scaffolds showed additional absorption bonds at 1644 and 1544 cm^{-1} in comparison with the other groups, indicating successful integration of NPY into the microporous scaffold. The mechanical tests did not show significant differences among the groups ($p > 0.05$). *In vitro* analyses showed that NPY was being released slowly from the TCP/Col/NPY scaffold, and the slow release was sustained for 20 days, with a cumulative release rate of 87.62 % $\pm$ 5.57 % at 20 days. The SD-BMSCs grew normally in the extract medium of the TCP/Col and TCP/Col/NPY groups. The CCK-8 cytotoxicity experiments showed that the TCP/Col/NPY microporous scaffold and TCP/Col were not cytotoxic. These results demonstrated that TCP/Col/NPY exhibits good biocompatibility.

In vivo, the TCP/Col/NPY group showed greater new bone formation at 30 and 60 d ($p < 0.05$) in the micro-CT scans. H&E and Masson staining revealed more new bone in the TCP/Col/NPY scaffold at 30 and 60 d ($p < 0.05$). Micro-CT and histopathological analyses suggested that NPY promoted new bone formation. These results were confirmed by the results of the immunohistochemical analyses. Runx2 and OCN are important markers of osteogenesis [33]. We detected Runx2 and OCN proteins in the connective tissue around the new bone undergoing bone remodeling in the microporous scaffold. The positivity rates of Runx2 and OCN were higher in the TCP/Col/NPY group ($p < 0.05$), consistent with the results for the NPY microporous scaffolds promoting bone formation.

However, these results contradicted with the unchanged ALP staining observed *in vitro*, suggesting that NPY is not directly responsible for the stronger osteogenic effect. Thus, NPY may promote osteogenic repair through other possible mechanisms. *In vitro*, TCP/Col/NPY showed greater angiogenesis-promoting activity than the other scaffolds in the tube-formation and HUVEC-migration assays. PDGF-BB is an important marker of tissue vascular regeneration [34]. Traditionally, vascular regeneration is closely associated with bone tissue regeneration. The presence of vascular regeneration in the scaffold indicated greater regenerative activity of the scaffold material. In this study, we found that the expression of PDGF-BB significantly increased in the TCP/Col/NPY group at 30 and 60 d. The promotion of local bone regeneration by NPY may be related to the promotion of angiogenesis in the scaffolds.

Macrophages play key roles in bone healing [35]. Macrophages are heterogeneous and plastic and play key roles in maintaining homeostasis and immune regulation. Macrophages can undergo M1 (pro-inflammatory) and M2 polarization (pro-healing), which play important roles in regulating the homeostasis of the tissue environment [36]. Among these, M2-type macrophages show good bone reconstruction and repair functions around the implant material, and can promote bone healing [37]. In this study, the markers of macrophage M1/M2 polarization were CD80 and CD206. *In vitro*, CD206 expression in RAW264.7 cells in the TCP/Col/NPY scaffold group was higher than that in the TCP and TCP/Col groups ($p < 0.05$). The proportion of M2 macrophage-polarized cells in the TCP/Col/NPY scaffold group was not significantly different from that in the interleukin-4 (IL-4)-induced positive control group. Meanwhile, iNOS levels were different among the three groups ($p > 0.05$). The results of the *in vitro* experiments predicted that NPY could promote M2 polarization of macrophages and had no effect on M1 polarization. *In vivo*, both CD80 and CD206 levels increased at 30 d and decreased at 60 d in the TCP/Col and TCP/Col/NPY groups ($p < 0.05$). However, the TCP/Col/NPY group showed higher levels of CD206 at 90 d ($p < 0.05$). Moreover, the CD206/CD80 ratio in the TCP/Col/NPY group was higher ($p < 0.05$). The results showed that the positive rate of M2-type macrophages in the TCP/Col/NPY group was higher, consistent with *in vitro* experiments. Thus, both *in vivo* and *in vitro* experiments demonstrated that NPY has a macrophage M2 polarization-promoting effect.

The TCP/Col/NPY microporous scaffold promoted both vascular regeneration and macrophage M2 polarization, but the link between vascular regeneration and macrophage M2 polarization remains unclear. The mechanisms underlying the actions of neurotransmitters in the osteogenic microenvironment are complex. Although previous research has mainly focused on promoting osteoblast differentiation, these results demonstrate that osteoblasts may promote osteogenesis through immune cell regulation and vascular regeneration. However, we found that the neurotransmitter NPY does not directly induce bone differentiation, and its osteogenesis-promoting effect, which may be initiated with NPY recruitment of macrophage M2 polar-

ization that may secrete vascular endothelial growth factor (VEGF) and promote blood vessel regeneration [38]. Then, macrophage M2 polarization promotes vascular regeneration and osteogenesis, but the mechanism needs to be further confirmed.

This study has several limitations that should be addressed in future research. As a neurotransmitter, NPY may exert biological effects beyond promoting osteogenesis, and its metabolic pathways in the body require further clarification. Future studies should also focus on developing bone repair materials capable of locally sustaining low-dose NPY release to enhance osteogenesis. In this study, NPY was shown to induce M2 macrophage polarization, leading to VEGF secretion and stimulation of angiogenesis. Nevertheless, the precise osteogenic mechanisms of NPY remain to be elucidated.

Conclusions

This study demonstrated that the TCP/Col/NPY microporous scaffold exhibits excellent histocompatibility and osteoinduction. *In vitro*, the TCP/Col/NPY microporous scaffold exhibited controlled release of NPY with no cytotoxicity. The TCP/Col/NPY microporous scaffold also exhibited excellent osteoinduction *in vivo*. In addition, more M2 macrophages were aggregated in the bone reconstruction tissue with the TCP/Col/NPY microporous scaffold. The TCP/Col/NPY microporous scaffold may be more conducive for recruiting M2-type macrophages into the scaffold or inducing M2 polarization of macrophages in the scaffold. The TCP/Col/NPY microporous scaffold also promoted vascular regeneration during bone repair. Thus, this scaffold shows potential as an artificial bone material that can be used for clinical bone-defect repair. However, the relationship between vascular regeneration and macrophage M2 polarization requires further investigation.

List of Abbreviations

β-TCP, β-tricalcium phosphate; NPY, neuropeptide Y; Col, collagen I; TGF-β, transforming growth factor-β; BMPs, bone morphogenetic proteins; SEM, scanning electron microscopy; FTIR, Fourier-transform infrared; SD-BMSCs, Sprague-Dawley rat bone marrow mesenchymal stem cells; HUVECs, human umbilical vein endothelial cells; CLSM, confocal laser scanning microscope; ALP, alkaline phosphatase; H&E, hematoxylin and eosin; PDGF-BB, platelet-derived growth factor-BB; OCN, osteocalcin; PI, propidium iodide; CCK, cell counting kit; PBS, phosphate-buffered saline; DMEM, Dulbecco's modified Eagle medium; iNOS, inducible nitric oxide synthase; CT, computed tomography; EDTA, ethylenediaminetetraacetic acid; BV, bone volume; TV, total volume; BMD, bone mineral density; ELISA, enzyme-linked immunosorbent assay; CD206, cluster of differentiation-206; VEGF, vascular endothelial growth factor; AM, acetoxymethyl ester.

Availability of Data and Materials

All data used or analysed in this study are available from the corresponding author on request.

Author Contributions

DZY, PL, ST, and WDH contributed to the design of the work. JT, ZX, and KH did the database search, screening, quality assessment, and data extraction. ZCC, CH, and WHY designed the experiments and workflow. ZCC and PL did the statistical analysis and interpreted the data. DZY and ZCC wrote the paper. PL, ZCC, JT, ZX, KH, CH, WHY, PL, ST, and WDH revised the manuscript critically; and all authors provided approval for publication of the content.

Ethics Approval and Consent to Participate

All procedures were approved by the Animal Experimental Ethics Committee of Shenzhen Huateng Biomedical Technology Co., Ltd. (B202402-5) and were conducted in accordance with the "Guide for the Care and Use of Laboratory Animals" published by the National Institutes of Health (NIH Publications No. 8023, revised 1978). All experimental procedures were conducted under the ARRIVE guidelines.

Acknowledgments

Not applicable.

Funding

This work was supported by grants from the Guangdong Basic and Applied Basic Research Foundation (2022A1515220036, 2023A1515220194), Natural Science Foundation of Guangdong Province (2514050000146), Medical Scientific Research Foundation of Guangdong Province (A2024380), Shenzhen Science and Technology Program (JSGG20210802153156021), Shenzhen Nanshan District Science and Technology Innovation Bureau Education (Health) Science and Technology funding project (NSZD2024019, NS2024011, NSZD2025003, NSZD2023036), and Futian District Health Research Project (FTWS 2022023, FTWS2025026).

Conflict of Interest

The authors have declared that no competing interest exists.

References

[1] Cheng X, Yao Y, Liu K, Wu L, Yang W. Free iliac crest grafting technology for the management of critical-sized tibial bone defect. BMC Musculoskeletal Disorders. 2024; 25: 201. https://doi.org/10.1186/s12891-024-07335-y.

[2] Seng DWR, Oh CW. Critical size bone defects managed with modern techniques of bone transport: An update. Injury. 2024; 55: 111341. https://doi.org/10.1016/j.injury.2024.111341.

[3] Deng Y, Zhou C, Fu L, Huang X, Liu Z, Zhao J, *et al*. A mini-review on the emerging role of nanotechnology in revolutionizing orthopedic surgery: challenges and the road ahead. Frontiers in Bioengineering and Biotechnology. 2023; 11: 1191509. https://doi.org/10.3389/fbioe.2023.1191509.

[4] Roddy E, DeBaun MR, Daoud-Gray A, Yang YP, Gardner MJ. Treatment of critical-sized bone defects: clinical and tissue engineering perspectives. European Journal of Orthopaedic Surgery & Traumatology: Orthopédie Traumatologie. 2018; 28: 351–362. https://doi.org/10.1007/s00590-017-2063-0.

[5] Fernandez de Grado G, Keller L, Idoux-Gillet Y, Wagner Q, Musset AM, Benkirane-Jessel N, *et al*. Bone substitutes: a review of their characteristics, clinical use, and perspectives for large bone defects management. Journal of Tissue Engineering. 2018; 9: 2041731418776819. https://doi.org/10.1177/2041731418776819.

[6] Shang L, Shao J, Ge S. Immunomodulatory Properties: The Accelerant of Hydroxyapatite-Based Materials for Bone Regeneration. Tissue Engineering. Part C, Methods. 2022; 28: 377–392. https://doi.org/10.1089/ten.TEC.2022.00111112.

[7] Luo P, Fang J, Yang D, Yu L, Chen H, Jiang C, *et al*. OP3-4 peptide sustained-release hydrogel inhibits osteoclast formation and promotes vascularization to promote bone regeneration in a rat femoral defect model. Bioengineering & Translational Medicine. 2022; 8: e10414. https://doi.org/10.1002/btm2.10414.

[8] Wan QQ, Qin WP, Ma YX, Shen MJ, Li J, Zhang ZB, *et al*. Crosstalk between Bone and Nerves within Bone. Advanced Science. 2021; 8: 2003390. https://doi.org/10.1002/advs.202003390.

[9] Reichmann F, Holzer P. Neuropeptide Y: A stressful review. Neuropeptides. 2016; 55: 99–109. https://doi.org/10.1016/j.npep.2015.09.008.

[10] Khor EC, Baldock P. The NPY system and its neural and neuroendocrine regulation of bone. Current Osteoporosis Reports. 2012; 10: 160–168. https://doi.org/10.1007/s11914-012-0102-7.

[11] Shi YC, Baldock PA. Central and peripheral mechanisms of the NPY system in the regulation of bone and adipose tissue. Bone. 2012; 50: 430–436. https://doi.org/10.1016/j.bone.2011.10.001.

[12] Liu S, Jin D, Wu JQ, Xu ZY, Fu S, Mei G, *et al*. Neuropeptide Y stimulates osteoblastic differentiation and VEGF expression of bone marrow mesenchymal stem cells related to canonical Wnt signaling activating *in vitro*. Neuropeptides. 2016; 56: 105–113. https://doi.org/10.1016/j.npep.2015.12.008.

[13] Gu XC, Zhang XB, Hu B, Zi Y, Li M. Neuropeptide Y accelerates post-fracture bone healing by promoting osteogenesis of mesenchymal stem cells. Neuropeptides. 2016; 60: 61–66. https://doi.org/10.1016/j.npep.2016.09.005.

[14] Çevik MÖ, Korkusuz P, Korkusuz F. Neuropeptide Y1 receptor antagonist but not neuropeptide Y itself increased bone mineral density when locally injected with hyaluronic acid in male Wistar rats. Turkish Journal of Medical Sciences. 2020; 50: 1454–1460. https://doi.org/10.3906/sag-2001-268.

[15] Nelson TS, Sinha GP, Santos DFS, Jukkola P, Prasoon P, Winter MK, *et al*. Spinal neuropeptide Y Y1 receptor-expressing neurons are a pharmacotherapeutic target for the alleviation of neuropathic pain. Proceedings of the National Academy of Sciences of the United States of America. 2022; 119: e2204515119. https://doi.org/10.1073/pnas.2204515119.

[16] Chen QC, Zhang Y. The Role of NPY in the Regulation of Bone Metabolism. Frontiers in Endocrinology. 2022; 13: 833485. https://doi.org/10.3389/fendo.2022.833485.

[17] Yunna C, Mengru H, Lei W, Weidong C. Macrophage M1/M2 polarization. European Journal of Pharmacology. 2020; 877: 173090. https://doi.org/10.1016/j.ejphar.2020.173090.

[18] Schlundt C, Fischer H, Bucher CH, Rendenbach C, Duda GN, Schmidt-Bleek K. The multifaceted roles of macrophages in bone regeneration: A story of polarization, activation and time. Acta Biomaterialia. 2021; 133: 46–57. https://doi.org/10.1016/j.actbio.2021.04.052.

[19] Movafagh S, Hobson JP, Spiegel S, Kleinman HK, Zukowska Z. Neuropeptide Y induces migration, proliferation, and tube formation of endothelial cells bimodally via Y1, Y2, and Y5 receptors. FASEB Journal: Official Publication of the Federation of American Societies for Experimental Biology. 2006; 20: 1924–1926. https://doi.org/10.1096/fj.05-4770fje.

[20] Zhao Y, Bai L, Zhang Y, Yao R, Sun Y, Hang R, *et al*. Type I collagen decorated nanoporous network on titanium implant surface promotes osseointegration through mediating immunomodulation, angiogenesis, and osteogenesis. Biomaterials. 2022; 288: 121684. https://doi.org/10.1016/j.biomaterials.2022.121684.

[21] Duan R, Zhang Y, van Dijk L, Barbieri D, van den Beucken J, Yuan H, *et al*. Coupling between macrophage phenotype, angiogenesis and bone formation by calcium phosphates. Materials Science & Engineering. C, Materials for Biological Applications. 2021; 122: 111948. https://doi.org/10.1016/j.msec.2021.111948.

[22] Qin Q, Lee S, Patel N, Walden K, Gomez-Salazar M, Levi B, *et al*. Neurovascular coupling in bone regeneration. Experimental & Molecular Medicine. 2022; 54: 1844–1849. https://doi.org/10.1038/s12276-022-00899-6.

[23] Jing X, Xu C, Su W, Ding Q, Ye B, Su Y, *et al*. Photosensitive and Conductive Hydrogel Induced Innerved Bone Regeneration for Infected Bone Defect Repair. Advanced Healthcare Materials. 2023; 12: e2201349. https://doi.org/10.1002/adhm.202201349.

[24] Appelt J, Baranowsky A, Jahn D, Yorgan T, Köhli P, Otto E, *et al*. The neuropeptide calcitonin gene-related peptide alpha is essential for bone healing. EBioMedicine. 2020; 59: 102970. https://doi.org/10.1016/j.ebiom.2020.102970.

[25] Zhang Z, Hao Z, Xian C, Fang Y, Cheng B, Wu J, *et al*. Neurobone tissue engineering: Multiple potential translational strategies between nerve and bone. Acta Biomaterialia. 2022; 153: 1–12. https://doi.org/10.1016/j.actbio.2022.09.023.

[26] Wu X, Wang Y, Wang H, Ma M, Hao Z, Ma Y. Neuropeptide Y regulates osteocyte phenotype and function through AHNAK-Smad signalling. Journal of Molecular Endocrinology. 2023; 71: e230011. https://doi.org/10.1530/jme-23-0011.

[27] Liu H, Wu J, Wu H, Wang T, Zhou H, Liu M. Autologous ADSCs with exogenous NPY promotes fracture healing in ovariectomized rats. Heliyon. 2024; 10: e38297. https://doi.org/10.1016/j.heliyon.2024.e38297.

[28] Reinke E, Fabry Z. Breaking or making immunological privilege in the central nervous system: the regulation of immunity by neuropeptides. Immunology Letters. 2006; 104: 102–109. https://doi.org/10.1016/j.imlet.2005.11.009.

[29] Chen WC, Liu YB, Liu WF, Zhou YY, He HF, Lin S. Neuropeptide Y Is an Immunomodulatory Factor: Direct and Indirect. Frontiers in Immunology. 2020; 11: 580378. https://doi.org/10.3389/fimmu.2020.580378.

[30] Long H, Ahmed M, Ackermann P, Stark A, Li J. Neuropeptide Y innervation during fracture healing and remodeling. A study of angulated tibial fractures in the rat. Acta Orthopaedica. 2010; 81: 639–646. https://doi.org/10.3109/17453674.2010.504609.

[31] Xie W, Li F, Han Y, Qin Y, Wang Y, Chi X, *et al*. Neuropeptide Y1 receptor antagonist promotes osteoporosis and microdamage repair and enhances osteogenic differentiation of bone marrow stem cells via cAMP/PKA/CREB pathway. Aging. 2020; 12: 8120–8136. https://doi.org/10.18632/aging.103129.

[32] Mohammad W, Chen L, Wu B, Dietz P, Bou-Akl T, Ren W, *et al*. Cell migration within porous electrospun nanofibrous scaffolds in a mouse subcuticular implantation model. Journal of Orthopaedic Research: Official Publication of the Orthopaedic Research Society. 2025; 43: 153–160. https://doi.org/10.1002/jor.25979.

[33] Lee JS, Lee JM, Im GI. Electroporation-mediated transfer of Runx2 and Osterix genes to enhance osteogenesis of adipose stem cells. Biomaterials. 2011; 32: 760–768. https://doi.org/10.1016/j.biomaterials

.2010.09.042.

[34] Gao SY, Lin RB, Huang SH, Liang YJ, Li X, Zhang SE, *et al*. PDGF-BB exhibited therapeutic effects on rat model of bisphosphonate-related osteonecrosis of the jaw by enhancing angiogenesis and osteogenesis. Bone. 2021; 144: 115117. https://doi.org/10.1016/j.bone.2019.115117.

[35] Weivoda MM, Bradley EW. Macrophages and Bone Remodeling. Journal of Bone and Mineral Research: the Official Journal of the American Society for Bone and Mineral Research. 2023; 38: 359–369. https://doi.org/10.1002/jbmr.4773.

[36] Chen X, Wan Z, Yang L, Song S, Fu Z, Tang K, *et al*. Exosomes derived from reparative M2-like macrophages prevent bone loss in murine periodontitis models via IL-10 mRNA. Journal of Nanobiotechnology. 2022; 20: 110. https://doi.org/10.1186/s12951-022-01314-y.

[37] Wang Y, Wang J, Gao R, Liu X, Feng Z, Zhang C, *et al*. Biomimetic glycopeptide hydrogel coated PCL/nHA scaffold for enhanced cranial bone regeneration via macrophage M2 polarization-induced osteo-immunomodulation. Biomaterials. 2022; 285: 121538. https://doi.org/10.1016/j.biomaterials.2022.121538.

[38] Yu Y, Dai K, Gao Z, Tang W, Shen T, Yuan Y, *et al*. Sulfated polysaccharide directs therapeutic angiogenesis via endogenous VEGF secretion of macrophages. Science Advances. 2021; 7: eabd8217. https://doi.org/10.1126/sciadv.abd8217.

Editor's note: The Scientific Editor responsible for this paper was Fergal O'Brian.

Received: 10th February 2025; **Accepted**: 26th November 2025; **Published**: 30th January 2026